Structure, tritium depth profile and desorption from 'plasma-facing' beryllium materials of ITER-Like-Wall at JET

E. Pajuste [a,*], G. Kizane [a], A. Vitins [a,b], I. Igaune [a,c], L. Avotina [a,c], R. Zarins [a,c], JET contributors [d,1]

[a] *Institute of Chemical Physics, University of Latvia, 1 Jelgavas St., Riga, LV-1004, Latvia*
[b] *Institute of Solid State Physics, University of Latvia, 8 Kengaraga st., Riga, LV-1063, Latvia*
[c] *Faculty of Chemistry, University of Latvia, 1 Jelgavas St., Riga, LV-1004, Latvia*
[d] *EUROfusion Consortium, JET, Culham Science Centre, Abingdon, OX14 3DB, UK*

ARTICLE INFO

ABSTRACT

Tritium depth profile and its temperature programmed desorption rate were determined for selected samples cut out of beryllium tiles removed from the Joint European Torus vacuum vessel during the 2012 shut down. A beryllium dissolution method under controlled conditions was used to determine the tritium depth profile in the samples, whereas temperature programmed desorption experiments were performed to assess tritium release pattern. Released tritium was measured using a proportional gas flow detector. Prior to desorption and dissolution experiments, the plasma-facing surfaces of the samples were studied by scanning electron microscopy and energy dispersive X-ray spectroscopy.

Experimental results revealed that $> 95\%$ of the tritium was localized in the top $30 - 45\,\mu m$ of the 'plasma-facing' surface, however, possible tritium presence up to $100\,\mu m$ cannot be excluded. During temperature programmed desorption at 4.8 K/min in the flow of purge gas $He + 0.1\%\ H_2$ the tritium release started below 475 K, the most intense release occurred at $725 - 915\,K$ and the degree of detritiation of $> 91\%$ can be obtained upon reaching 1075 K. The total tritium activity in the samples was in range of 2 $- 32$ kilo Becquerel per square centimetre of the plasma-facing surface area.

1. Introduction

Currently the ITER-Like-Wall (ILW) project is being carried out at Joint European Torus (JET). This project aims to test materials relevant to ITER (International Thermonuclear Experimental Reactor). The first wall of the vacuum vessel is made of bulk beryllium and beryllium coated inconel tiles, whereas for the divertor bulk tungsten and tungsten coated carbon fibre composite tiles are used [1].

Performance of the wall materials is mostly limited by the surface erosion and tritium retention. Long term fuel retention is not only economical but also radiological issue due to radioactivity of tritium.

There have been number of separate experiments with deuterium-tritium mixtures in which tritium have been introduced in JET. Most recent tritium experiment was performed in 2003 - Trace Tritium Experiment –TTE [2]. Tritium has not been introduced within ILW campaign yet, however tritium has remained in the vacuum vessel since D-T experiments; moreover it can be produced in the D-D reactions and also in the beryllium reactions with neutrons themselves.

Tritium accumulation in wall materials can occur as a result of its co-deposition with eroded particles and implantation/diffusion in the bulk of the wall materials.

Aim of this study is to assess tritium accumulation in the beryllium wall materials and factors affecting it. Tritium content, its depth profile and thermal desorption pattern were studied, as well as structure and chemical composition of the 'plasma-facing' surface.

2. Experimental

2.1. Samples investigated

In this study, tiles exposed in JET during the first year of JET-ILW operation (2011–2012) were analysed. During this period total
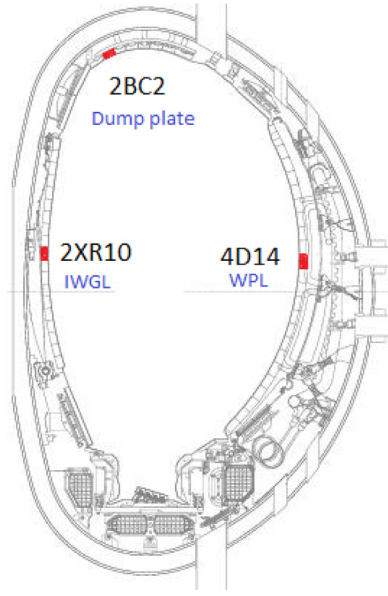

Fig. 1. Position of the analysed samples in vacuum vessel.

operational time was 19 h including dedicated discharges in limiter configuration to assess Be erosion [3]. During the shutdown that followed the first ILW campaign, a number of tiles were retrieved for post-exposure analysis. Tiles used in this study were from the upper region (Upper Dump Plate) and mid-region (inner wall - Inner Wall Guard Limiter (IWGL), and outer -Wide Poloidal Limiter (WPL)) of the vessel (Fig. 1).

Samples of approximately $1.2 \times 1.2 \times 1.0\,cm^3$ cut out of tiles (as described in [4]) were used in the present study. These samples were further cut into two parts in order to perform tritium depth profiling and desorption experiments. During cutting of the samples, their temperature was controlled not to exceed ~60 °C in order to avoid tritium loss as a result of thermal desorption.

2.2. Surface structure and chemical composition analysis

Methods of scanning electron microscopy (SEM) and energy dispersive X-ray spectroscopy (EDX) were used for surface structure and chemical composition analysis. Scanning electron microscope *Hitachi S-4800* and EDX detector *Quantax Esprit 1.9* were used in this study.

2.3. Determination of tritium depth profile

Tritium (depicted as 'T') depth profile was measured by the means of dissolution method developed for tritium measurement in bulk beryllium. In this method, successive layers of Be were removed using 1 mol/L sulphuric acid and amount of evolved hydrogen (depicted as 'H') and released tritium were measured. Following processes are taking place during the dissolution:

$$Be^0 + 2H^+ \rightarrow Be^{2+} + 2H^0 \tag{1}$$

$$H^0 + H^0 \rightarrow H_{2(gas\ ph.)} \tag{2}$$

$$H^0 + T^0_{(solid\ phase)} \rightarrow HT_{(gas\ ph.)} \tag{3}$$

$$T_{2(solid\ ph.)} \rightarrow T_{2(gas\ ph.)} \tag{4}$$

$$T^+_{(solid\ ph.)} \rightarrow T^+_{(liquid\ ph.)} \tag{5}$$

where, '$T^0_{(solid\ phase)}$' refers to tritium atoms as interstitials in the bulk of solid beryllium, '$T_{2(solid\ ph.)}$' - molecular tritium trapped in the bulk of the solid beryllium, '$T^+_{(solid\ ph.)}$' – tritium chemically bonded with the impurities in the bulk of solid beryllium, whereas '$T_{2\ (gas\ ph.)}$' – molecular tritium released in the flow of the purge gas and '$T^+_{(liquid\ ph.)}$' - tritium remaining in the acid solution as a part of the HTO^+ ion. In the 1 mol/L sulphuric acid molecular T_2 and atomic T^0 (interstitial) tritium of the activities A_{T2} and A_{T0} respectively, present in a Be sample transfer as $T_2 + HT$ into a flow of carrier gas, where the tritium activity was measured by proportional counter with an operating volume of 300 cm^3 and a tritium monitor TEM 2102A [Mab Solutions GmbH].

$$A_{T,\ gas\ ph} = A_{T2} + A_{T0} \tag{6}$$

Chemically bonded tritium (depicted as 'T^+' in the processes schemes) localized in a Be layer remains in the solution and the tritium activity $A_{T,\ liquid\ ph.}$ was measured with liquid scintillation method. Solution containing tritium was distilled and 5 mL aliquot mixed with 15 mL of Ultima Gold scintillation cocktail and analysed for total tritium with a TRi-Carb 2910TR counter [PerkinElmer, Inc].

Amount of tritium atoms can be calculated by means of the tritium decay constant $\lambda = 1{,}78\ 10^{-9}\,s^{-1}$ [5]

$$N_T = \frac{A_T}{\lambda} \tag{7}$$

Calculations on tritium distribution in the bulk of the sample are based on the controlled dissolution process. One hydrogen molecule corresponds to one beryllium Eqs. (1) and ((2)) atom and the dissolution rate of beryllium and hereby also the thickness of dissolved layer L_t at the moment t can be calculated from the number hydrogen molecules evolved, $N_{H2,t}$.

$$L_t = \frac{N_{H_2,t} \cdot M_{Be}}{N_A \cdot \rho_{Be} \cdot S_{Be,\ dis}} \tag{8}$$

where M_{Be}- beryllium atomic mass (9.012 u), N_A –Avogadro constant (6.022·10^{23} mol^{-1}), ρ_{Be}- beryllium theoretical density (1.85 g/cm^3) and $S_{Be,\ dis}$(cm^2) - surface area of the beryllium sample being etched by the acid.

Hydrogen amount were measured by the means of gas chromatography using thermal conductivity detector (TCD). By this method all hydrogen isotopes are measured as one signal, however tritium and deuterium concentrations are very low if to compare with the amount of protium evolved during beryllium dissolution process.

Tritium concentration (atomic parts per million appm) in the sample is calculated as the ratio of released tritium atoms and dissolved beryllium in the time period Δt.

Resolution of this is determined by the sample properties (porosity, grain size), geometry of the setup (volumes of the dissolution cell, the column filled with silica gel and tritium detector), the flow rate of the argon carrier gas and the rate of dissolution of the beryllium sample in 1 mol/L sulphuric acid. For particular samples resolution is limited by the non-uniform dissolution of the material. Additional experiments were performed where samples were removed from the solution and SEM analysis of the acid exposed surface performed. This analysis revealed surface roughness with the maximum roughness height up to 10 μm. Therefore the resolution was assumed to be ~10 μm. Depth profile graphs are constructed from the tritium and hydrogen measurement data and are precise in case of smooth solution process.

2.4. Thermal desorption of tritium

Thermal desorption of tritium was performed in a flow of He + 0.1% H$_2$ purge gas at 14–15 L/h.The quartz tube in the setup

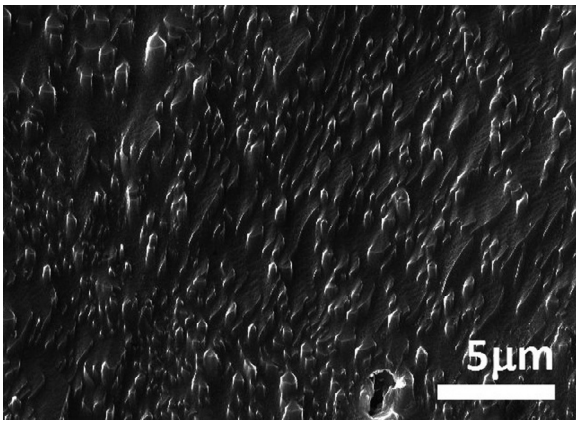**Fig. 2.** SEM micrographs of sample No 41 showing prolonged beryllium structures.

Fig. 3. SEM micrograph of sample No 60 showing scale like deposition layer.

had two compartments – one for the sample in a porcelain boat and one for a bed of granulated zinc. The quartz cap had a thermocouple channel – an inner quartz tube sealed towards the sample. The zinc bed at 665–675 converts tritiated water to molecular gaseous tritium (HT, DT, and traces of T_2). Samples were heated at a rate of 4.8 K/min to 1305 K and then kept at that temperature for 1 h. The temperatures of the sample, the zinc bed and the cold trap were continuously measured. The tritium activity in the purge gas was continuously monitored using a proportional counter with an operating volume of 300 cm^3 and a tritium monitor TEM 2102A. The total released tritium activity was calculated by integrating the release rate over the time where a release was measurable. The radioactivity of tritium released was calculated as kBq/cm^2 to 1 cm^2 of the plasma-facing surface area of the sample. As the subsequent second heating of the same sample in the same setup with the same temperature program to 1303 K caused no appreciable tritium release, the final value of the tritium sum release in the first heating was defined as a total tritium release. As most of tritium released during the temperature ramp of 4.8 K/min to 1305 K, the release rate and the sum release were plotted as functions of temperature.

3. Results

3.1. Surface structure and chemical composition

Analysis of the surface was performed to estimate effects of the conditions the samples have been exposed to - if there has been any melting, plasma etching or formation of deposition layer.

Inner Wall Guard limiter IWGL

Results of SEM and EDX analysis revealed that surface of central part of the tile (sample 41) is comparably clean (almost no deposition). Prolonged beryllium structures can be observed (Fig. 2) that might indicate the plasma induced erosion. Similar surface morphology has been reported after light ion plasma exposure of beryllium in plasma device Pisces-B [6].

Outer part of the tile (samples 60, 28) have surface coated with a deposition layer of "scale like" structure (Fig. 3). According to EDX data deposition layer contains nickel, oxygen, carbon and traces of tungsten and iron.

Wing part of the tile (samples 14 and 75) has "cabbage like" deposition layer with melted/resolidified beryllium droplets on the surface of it. Irregular and prolonged shape droplets of melted and then solidified beryllium can be found randomly on the surface of the deposition layer (Fig. 4). These droplets of the beryllium have a micro/nano scaled porosity. The structure of the melted beryllium corresponds well to the results on exposing Be to the plasma loads outside the vessel [7].
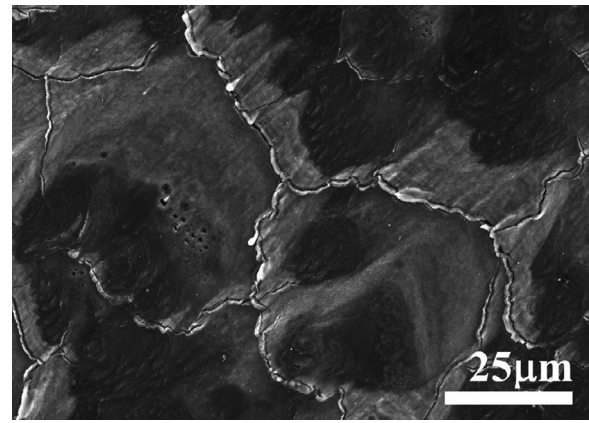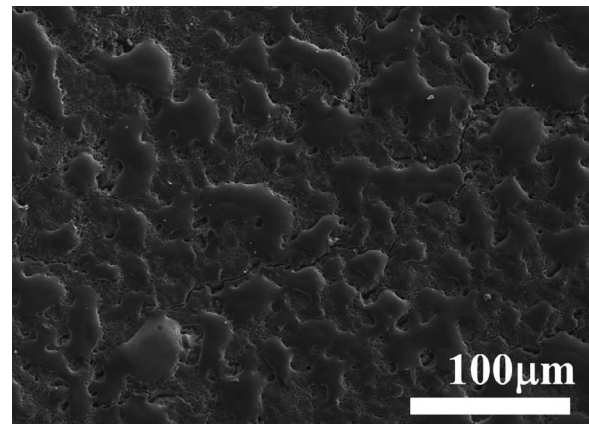

Fig. 4. SEM micrograph of sample No 75 showing melted/resolidified beryllium droplets.

In the erosion studies at JET strong melting has been described in the mid-plane region on inner limiter and this part is a net erosion zone as a result of interaction with limiter plasmas. It corresponds well to the structure of the central part of the tile. Moreover, this molten material has travelled in an upward poloidal direction due to jxB Lorentz forces and plasma pressure [8]. It might explain the prolonged shape of the molten beryllium droplets.

Wide Poloidal Limiter WPL

Results of the SEM and EDX analysis revealed that surface of the central part of the tile from WPL (sample 130) has similar prolonged beryllium structures as were observed on the central part of the tile from IWGL 2XR10 (sample no. 41). However, above these structures a deposition layer is present. It might indicate that plasma induced erosion of beryllium was less intense and was followed by lower temperature regime when deposition layer was formed.

Outer part of the tile has a deposition layer with microparticles of high nickel concentration on the surface of it. Moreover these particles are deposited on the surface in a specific pattern - as parallel lines that are visible also by a naked eye (Fig. 5). Nickel has been used as a marker for erosion studies previously, therefore these particles originates from marked tiles near the studied one.

Samples from the left and right wings of the tile (no. 106 and 165) are covered with the layer of melted/resolidified beryllium. This layer has cracks and bubbles from which part has "exploded". Moreover, in areas of the bubbles, increased oxygen content was observed. Resolidified beryllium layer is partly delaminated from
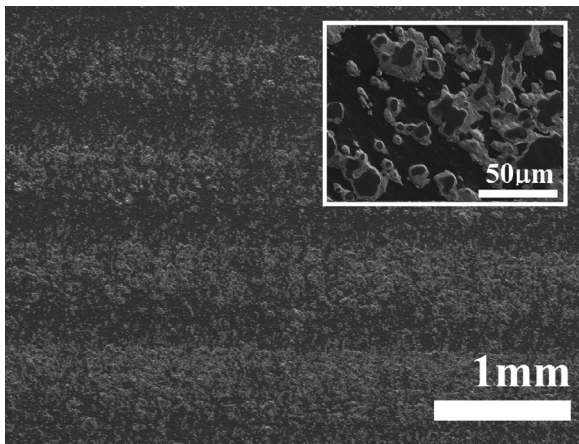
Fig. 5. SEM micrograph of sample No 114 showing microparticles of high nickel content organized as parallel lines.

the sample no. 106 and reveals a layer of comparably high nickel content below it.

Upper Dump Plate

Surface structure of the sample from outer part of the Upper Dump Plate tile is similar to the structure of inner wall tile outer part. Surface is covered by the "cabbage like" deposition layer with melted beryllium droplets on it.
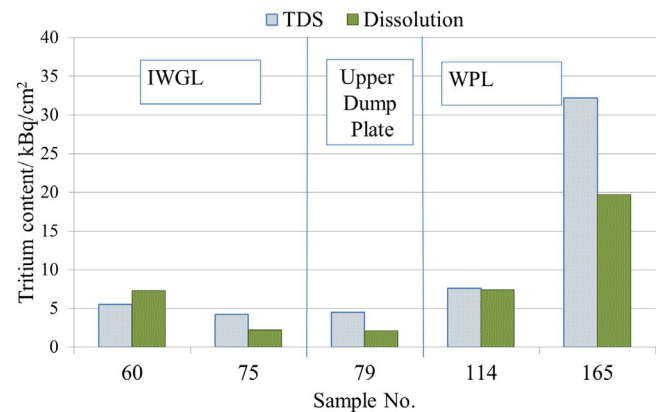
3.2. Tritium content

Each sample was cut into two parts in order to perform tritium depth profiling and desorption experiments. Both methods give also information on tritium total content in the sample. A possible non-uniform tritium distribution across the plasma-facing surface of the sample can be a reason that the T amount measured is not equal in both parts of the sample. Moreover, it can be assumed that more precise values give thermal desorption results since they include also tritium accumulated in the deposition layer. Summary of tritium content is given in the Table 1.

Results revealed that higher tritium concentrations can be found in the samples from the outer wall (WPL). In the WPL samples tritium content was from 7.5 kBq/cm^2 (4.2×10^{12} atoms/cm^2) in sample 114–32.3 kBq/cm^2 (18.1×10^{12} atoms/cm^2) in 165,

Table 1
Tritium content in samples measured by the methods of dissolution and thermal desorption.

| Tile	Position in tile	Sample no	Tritium content, kBq/cm^2		
			Dissolution	TDS	Average
IWGL	Outer	60	7.5	5.5	6.4
	Wing	75	2.2	4.2	3.2
WPL	Center	130	14.5	–	14.5
	Outer	114	7.4	7.5	7.5
	Wing	165	19.7	32.3	26.0
Dump Plate	Outer	79	2.1	4.5	3.3

Fig. 6. Tritium content in beryllium samples from IWGL (60, 75), Upper Dump Plate (79) and WPL (114, 165).

whereas in the IWGL samples highest concentration was found to be 7.5 kBq/cm^2 (4.2×10^{12} atoms/cm^2) in sample 60. In the sample from Upper Dump Plate tritium concentration was 4.5 kBq/cm^2 (2.5×10^{12} atoms/cm^2) (Fig. 6).

3.3. Tritium depth profile

Tritium depth profile measurement shows that 95% of tritium is accumulated in the first 30 – 45 µm from the 'plasma-facing' surface. In the sample of high tritium content – 165 from the WPL, low concentration of tritium can be found up to 100 µm (Fig. 7).
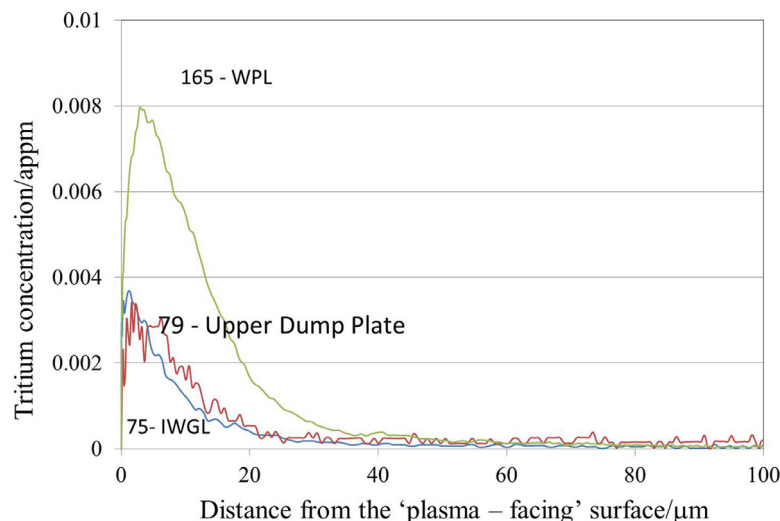
Fig. 7. Tritium depth profile of beryllium samples 75 from IWGL (blue), 165 from WPL (green) and 79 from Upper Dump Plate (red). (For interpretation of the references to colour in this figure legend, the reader is referred to the web version of this article.)
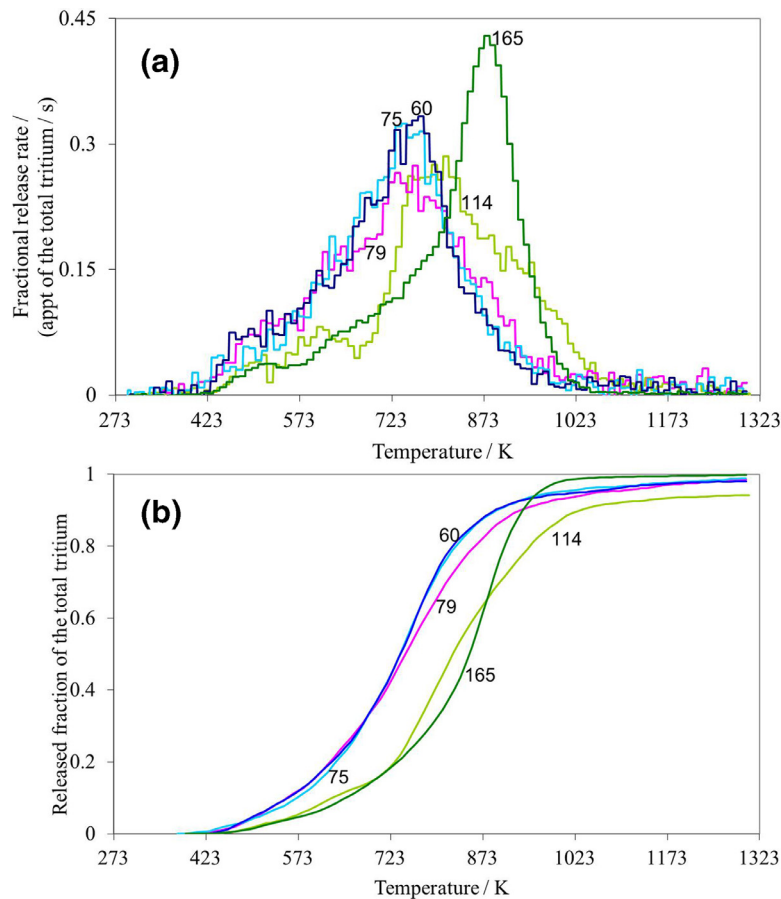
Fig. 8. Spectra of temperature-programmed desorption of tritium at the rate of temperature increase of 4.8 K/min for the samples having respective final values of the tritium sum release for 1 cm^2 of the plasma-facing surface area: sky blue curves – sample 75 of IWGL; dark blue curves – sample 60 of IWGL; pink curves – sample 79 of the Upper Dump Plate; lime curves – sample 114 of WPL; green curves – sample 165 of WPL. The atomic parts per thousand (appt) in Fig. 11a have been calculated with respect to the final values of the tritium sum release for 1 cm^2 of the plasma-facing surface area for each sample. (For interpretation of the references to colour in this figure legend, the reader is referred to the web version of this article.)

3.4. Tritium thermal desorption

Though the values of the total tritium content of the samples are quite different, their tritium release patterns can be clearly compared by calculating and plotting their tritium release rate and sum release as fractions with respect to their final values of the tritium sum release. Curves thus obtained for the tritium release rate and sum release are shown in Fig. 8a and b respectively.

Samples 60 and 75 of IWGL and sample 79 of the Upper Dump Plate had their total tritium content in the range 4.2–5.5 kBq/cm^2, but their fractional release rate and released fraction as functions of temperature were quite similar (Fig. 8). Their curves of the fractional release rate had a single distinct maximum: the tritium release started at 375–425 K, reached its maximum rate at 725–775 K, and, upon reaching 1025 K, more than 93% of the total tritium were released. Sample 79 of the Upper Dump Plate had a slightly broader maximum and more gradual descent of the fractional tritium release rate than samples 60 and 75 of IWGL (Fig. 8).

It is evident from Fig. 8 that samples 114 and 165 of WPL had tritium release patterns that differ from those of samples 60 and 75 of IWGL and that of sample 79 of the Upper Dump Plate. Though the tritium release started also at 375–425 K, the fractional tritium release rate of samples 114 and 165 of WPL had a distinct shoulder at 425–675 K (sample 114) or at 425–775 K (sample 165) that preceded the main maximum at 735 – 835 K (sample 114) or at 835 – 915 K (sample 165). Sample 114 had a more gradual descent of the fractional tritium release rate than sample 165 in the

temperature range of 975 –1125 K. Upon reaching 1075 K, the degree of detritiation of all the samples investigated was more than 91%.

4. Discussion

Results of structural analysis show that there has been plasma induced erosion from the central part of the IWGL and WPL tiles and melted material has transferred to the sides of the tiles where it has resolidified. Comparison of the tritium concentration in different positions on the tile reveals that there is less tritium in plasma wetted regions and its highest concentration can be found in the regions where melted material is present. For example, sample from the central part of the WPL tile that has evidences of direct plasma impact contains 7.5 kBq/cm^2 of tritium, whereas it's outer part with deposition layer and resolidified beryllium – 32.3 kBq/cm^2. Tritium accumulation depends also on the tile position in the vacuum chamber – it is more intense in the outer wall tiles than that in the upper region or inner wall. These results correspond well to the measured deuterium concentration by other authors [9]. Moreover, tritium desorption experiments showed that maximum release rate for samples from the outer wall is reached at higher temperatures. However, degree of 90% detritiation is reached at 1040 °C for all the samples investigated in the present study.

Tritium thermo-desorption from neutron irradiated beryllium had been analysed widely in order to get comprehensive overview

of the processes occurring during high temperature treatment [10–16]. However, in 'plasma-facing' beryllium materials from ILW campaign tritium accumulation is dominated by the co-deposition and direct implantation of ions, diffusion and migration into the bulk [17,18]. Temperature required to reach material detritiation differs significantly depending on the tritium accumulation pathway. For example, tritium desorption from pebbles in which tritium is loaded by thermo- sorption process occurs at much lower temperatures than that from neutron irradiated pebbles of the same production batch [19–20]. Depth profiles of plasma exposed and neutron irradiated beryllium demonstrates that in neutron irradiated beryllium tritium is accumulated within all the bulk of material [21], whereas in plasma exposed - only in the surface layer up to 100 μm. Moreover, in neutron irradiated beryllium most tritium is trapped in the helium inclusions. Therefore, tritium desorption from 'plasma-faced' beryllium from JET occurs at lower temperature - desorption starts at ~375 K if to compare with ~800 K of neutron irradiated beryllium [22]. In ITER where significant neutron fluxes will be present tritium accumulation and its thermal desorption is expected to be more complex and required temperature for detritiation of 'plasma-facing' materials could be higher that determined in this study.

5. Conclusions

- Tritium content is higher in the outer wall Be limiter tiles (7.5–32.3 kBq/cm^2) than that in inner wall and upper region tiles (4.1 −7.5 kBq/cm^2).
- Plasma - wetted regions contain less tritium, highest tritium concentrations can be found in areas where melted beryllium from these regions has been transferred.
- Tritium desorption from beryllium samples started at 375–425 K, had a maximum rate at 725–915 K, and at 1075 K the degree of detritiation was more than 91%.
- Tritium desorption patterns of samples from the outer wall Be limiter tiles are significantly different from those of samples from the inner wall and upper region tiles.
- 95% of tritium is accumulated in the first 30 - 45 μm, however, possible presence of tritium in low concentration up to the depth of 100 μm cannot be excluded.

Acknowledgements

References

[1] G.F. Matthews, M. Beurskens, S. Brezinsek, M. Groth, E. Joffrin, A. Loving, M. Kear, M.L. Mayoral, R. Neu, P. Prior, V. Riccardo, F. Rimini, M. Rubel, G. Sips, E. Villedieu, P.d. Vries, M.L. Watkins, EFDA JET contributors, Physica Scripta T145 (2011) 014001.
[2] T.T.C. Jones, EFDA JET Contributors, Fusion Sci. Technol. 48 (2005) 250–257.
[3] S. Brezinsek, J. Nucl. Mater. 463 (2015) 11–21.
[4] A. Widdowson, A. Baron-Wiechec, P. Batistoni, E. Belonohy, J.P. Coad, P. Dinca, D. Flammini, F. Fox, K. Heinola, I. Jepu, J. Likonen, S. Lilley, C.P. Lungu, G.F. Matthews, J. Naish, O. Pompilian, C. Porosnicu, M. Rubel, R. Villari, JET Contributors, Physica Scripta 2016 (2016) 014057.
[5] L.L. Lucas, M.P. Unterweger, J. Res. Natl. Inst. Stand. Technol. 105 (4) (2000) 541–549.
[6] R.P. Doerner, M.J. Baldwin, D. Nishijima, J. Nucl. Mater. 455 (2014) 1–4.
[7] I.B. Kupriyanov, G.N. Nikolaev, L.A. Kurbatova, N.P. Porezanov, V.L. Podkovyrov, A.D. Muzichenko, A.M. Zhitlukhin, A.A. Gervash, V.M. Safronov, J. Nucl. Mater. 463 (2015) 781–786.
[8] A. Widdowson, E. Alves, C.F. Ayres, A. Baron-Wiechec, S. Brezinsek, N. Catarino, J.P. Coad, K. Heinola, J. Likonen, G.F. Matthews, M. Mayer, M. Rubel, JET Contributors, Physica Scripta 2014 (2014) 014010.
[9] K. Heinola, A. Widdowson, J. Likonen, E. Alves, A. Baron-Wiechec, N. Barradas, S. Brezinsek, N. Catarino, P. Coad, S. Koivuranta, S. Krat, G.F. Matthews, M. Mayer, P. Petersson, JET Contributors, Physica Scripta 2016 (2016) 014075.
[10] E. Rabaglino, C. Ronchi, A. Cardella, Fusion Eng. Des. 69 (2003) 455–461.
[11] D.L. Baldwin, M.C. Billone, J. Nucl. Mater. 212-215 (1994) 948–953.
[12] F. Scaffidi-Argentina, M. Dalle Donne, H. Werle, Fusion Eng. Des. 58–59 (2001) 641–645.
[13] F. Scaffidi-Argentina, M. Dalle Donne, H. Werle, J. Nucl. Mater. 258–263 (1998) 595–600.
[14] I.B. Kupriyanov, G.N. Nikolaev, V.V. Vlasov, A.M. Kovalev, V.P. Chakin, J. Nucl. Mater. 367–370 (Part A) (2007) 511–515.
[15] A.V. Fedorov, S. van Til, L.J. Magielsen, M.P. Stijkel, J. Nucl. Mater. 442 (1–3) (2013) S472–S477 Supplement 1.
[16] E. Pajuste, G. Kizane, L. Avotina, A. Zarins, J. Nucl. Mater. 465 (2015) 293–300.
[17] G. Federici, et al., Plasma-material interactions in current tokamaks and their implications for next step fusion reactors, Nucl. Fusion 41 (12) (2001) 1967.
[18] A.A. Pisarev, M.L. Grachova, Plasma-driven accumulation of tritium in beryllium, J. Nucl. Mater. 233–237 (Part 2) (1996) 1137–1141.
[19] V. Chakin, A. Moeslang, P. Kurinskiy, R. Rolli, H.C. Schneider, E. Alves, L.C. Alves, Fusion Eng. Des. 86 (9–11) (2011) 2338–2342.
[20] A. Vitins, V. Zubkovs, G. Kizane, E. Pajuste, V. Kinerte, Fusion Sci. Technol. 60 (3) (2011) 1143–1146.
[21] J. Tiliks, G. Kizane, A. Vitins, E. Kolodinka, V. Tilika, B. Lescinskis, Nucl. Technol. 159 (3) (2007) 245–249.
[22] A. Vitins, G. Kizane, A. Matiss, E. Pajuste, V. Zubkovs, J. Nucl. Mater. 442 (1–3) (2013) S490–S493.